Tactile Sensing Cube Measuring Stress Tensor

Shohei Kiyota[1] and Hiroyuki Shinoda[2]

Department of Department of Information Physics and Computing, The University of Tokyo, Tokyo, Japan
[1] (Tel : +81-3-5841-6927; E-mail: kiyot@alab.t.u-tokyo.ac.jp)
[2] (Tel : +81-3-5841-6926; E-mail: shino@alab.t.u-tokyo.ac.jp)

Abstract: We propose a tactile sensing cube that is a rectangular rigid body with symmetrically-located stress sensors and embedded in an elastic body. The sensor measures stress tensor applied to the elastic body and can distinguish between shear and non-uniformly distributing normal stress applied to the surface of the body. The previously reported tactile sensors could not distinguish these stresses. In this paper, we verify the detection principle qualitatively by FEM simulation of two dimensional model and we show the result of basic experiments using a prototype.

Keywords: tensor sensor, force sensor, symmetrical, elastic body

1. INTRODUCTION

A sensor chip that is available in an elastic body to measure the stress tensor is desired in wide variety of application fields that need the information of contact to objects (e.g. robot skin, shoe sole, etc…) [1],[2]. The previously reported tensor sensors had pairs of normal stress sensing elements in order to estimate the shear stress [2]. However, they have sensitivity to not only shear stress but also non-uniformly distributing normal stress.

In this paper, we propose a new cube-type tactile sensor embedded in an elastic body. It measures surface stress tensor applied to the body. This cube has normal stress sensors located on each side of the cube as shown in Fig. 1, and can distinguish between non-uniformly distributing normal stress and shear stress.
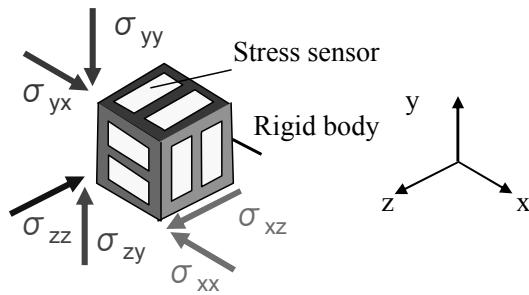

Fig. 1 Tactile Cube

2. PRINCIPLE

As described in Section 1, one major shortcoming of conventional tensor sensors is that they were not able to distinguish between non-uniformly distributing normal stress and shear stress [2]. They calculated normal stress by the average of the sub-sensor's output and shear stress by the difference. However, they have sensitivity to not only shear stress but also non-uniformly distributing normal stress as shown in Fig.2.

Our method utilizes the symmetric structure of the cube to overcome the shortcoming. In this section, the principle of the proposed stress tensor sensor is explained using a simple model.

The stress tensor sensor consists of a cube-shaped rigid body and normal stress sensors placed on each side. It is embedded in a linear elastic body. For simplification, the following discussion focuses on a cross section including the x- and z-axis as shown in Fig. 3.

From the symmetry, the relationship of the normal stress sensor's output in the elastic body V_1, V_2, V_3, V_4, V_5, V_6, V_7, V_8 to input stress tensor applied to the surface of the body σ_{zz}, σ_{zx}, σ_{xx}, σ_{xz}, and gradient of normal stress $\partial\sigma_{zz}/\partial x$, $\partial\sigma_{zz}/\partial z$, $\partial\sigma_{xx}/\partial z$, $\partial\sigma_{xx}/\partial x$ applied to the surface are expressed as

$$
\begin{pmatrix} V_1 \\ V_2 \\ V_3 \\ V_4 \\ V_5 \\ V_6 \\ V_7 \\ V_8 \end{pmatrix} =
\begin{pmatrix}
a & -c & -b & -d & -e & -g & f & h \\
a & c & -b & d & e & -g & f & -h \\
a & c & -b & d & -e & g & -f & h \\
a & -c & -b & -d & e & g & -f & -h \\
-b & -d & a & -c & f & h & -e & -g \\
-b & d & a & c & f & -h & e & -g \\
-b & d & a & c & -f & h & -e & g \\
-b & -d & a & -c & -f & -h & e & g
\end{pmatrix}
\begin{pmatrix}
\sigma_{zz} \\ \sigma_{zx} \\ \sigma_{xx} \\ \sigma_{xz} \\
d_0\dfrac{\partial\sigma_{zz}}{\partial x} \\
d_0\dfrac{\partial\sigma_{zz}}{\partial z} \\
d_0\dfrac{\partial\sigma_{xx}}{\partial z} \\
d_0\dfrac{\partial\sigma_{xx}}{\partial x}
\end{pmatrix}
\quad (1)
$$

with constants $a,\ b, ... , g,$ and h.

As a result, we can reconstruct the stress applied to the elastic body without the affection of the other component.

$$
\sigma_{zz} = \frac{a}{4(a^2-b^2)}\left(\sum_{i=1}^{4}V_i + \frac{b}{a}\sum_{i=5}^{8}V_i\right), \qquad (2)
$$

$$
\sigma_{xx} = \frac{a}{4(a^2-b^2)}\left(\sum_{i=5}^{8}V_i + \frac{b}{a}\sum_{i=1}^{4}V_i\right), \qquad (3)
$$

$$
\sigma_{zx} = \sigma_{xz} = \frac{1}{8(c+d)}(V_1 - V_2 - V_3 + V_4). \qquad (4)
$$

In addition, gradient of the normal stress applied to the top surface of the elastic body "$\partial\sigma_{zz}/\partial x$" is reconstructed as

$$\frac{\partial \sigma_{zz}}{\partial x} = \frac{h}{4(eg - fh)}\left\{(-V_1 + V_2 - V_3 + V_4)\right.$$
$$\left. - \frac{g}{h}(V_5 + V_6 - V_7 - V_8)\right\} \quad (5)$$

The other components of normal stress gradient are also obtained by the similar procedures.
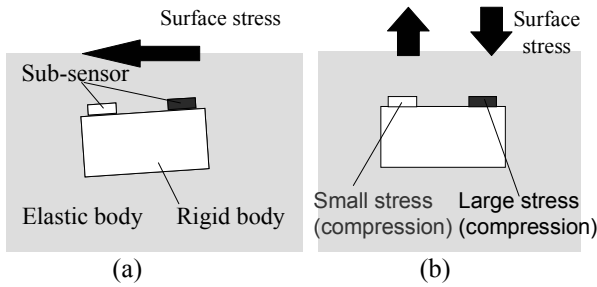

Fig. 2 The problem of the previously reported stress tensor sensor. The rigid body and two normal stress sensors are embedded in an elastic body. This tensor sensor outputs the difference between outputs of sub-sensor as shear stress. Both (a) applied shear stress to the surface of the elastic body and (b) applied non-uniformly distributing normal stress are detected as shear stress.
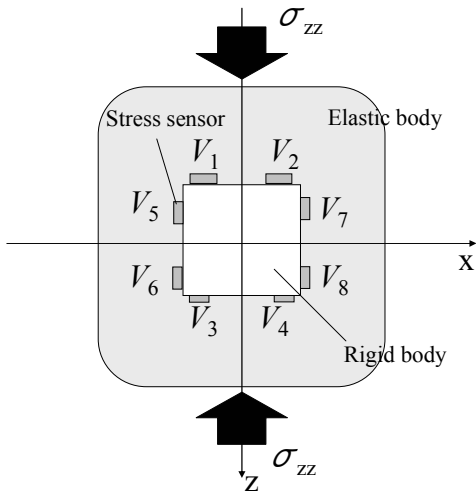

Fig. 3 Schematic drawing of the sensor model. The white square indicates the rigid body. The length of each side of the square is $2d_0$. Normal stress applied to the elastic body "σ_{zz}" acts on V_1, V_2, V_3 and V_4 equally. The same goes for V_5, V_6, V_7 and V_8.

3. FEM SIMULATION

To confirm the validity of the model discussed in Section 2, FEM simulations were carried out. A steel rigid cube (Young's modulus 200 GPa and Poisson's ratio 0.30) was embedded in a silicone rubber with the Young's modulus of 0.3MPa and the Poisson's ratio of 0.48. The thickness of the silicone rubber was 11 mm and the width was 60 mm. The length of each side of the cube was 4 mm. The cube was placed at the center of the silicone rubber.

The results are shown in Fig. 4. The intensity of the z-component of the normal stress is plotted. Fig. 4 (a) shows the results for the case in which only the shear stress is applied on the surface of the linear elastic body. Fig. 4 (b) is the result for the case in which the normal stress distribution is applied on the surface of the linear elastic body. In the case of Fig. 4 (b), the intensity of the applied normal stress was varied linearly along the x-axis.

In Fig. 4 (a), around the lower left side and upper right side of the rigid square, the elastic body was stretched. In contrast, around the upper left side and lower right side of the rigid square, the compressed region was observed. These results back up the symmetrical property of the coefficient matrix discussed in the previous section.
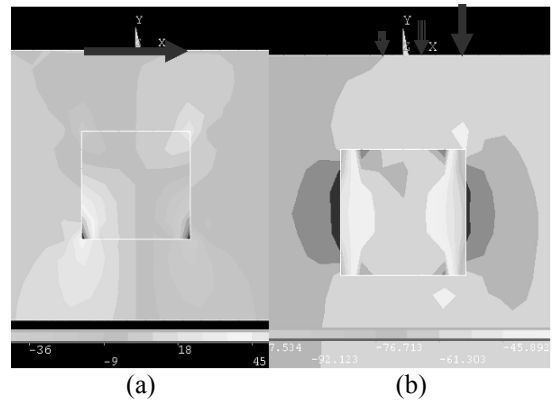

Fig. 4 Simulation results. Arrows on the surface of the silicone rubber represent applied force. (a) Applied shear stress and (b) linearly varied normal stress

4. EXPERIMENTS

4.1 Prototype

We fabricated a tactile sensing cube (Fig. 5) and embedded it in a soft silicone rubber. The cube consists of an acrylic cube and four capacitive stress sensors placed on the corner of the cube. Each capacitive stress sensor consisted of two copper electrodes and urethane foam. One of the electrodes was connected to GND and the other was connected to the input of a Schmitt inverter so that Schmitt inverter oscillator was formed. The prototype sensor was embedded in a silicone rubber. The frequency of the RC oscillator was specified by the ca-

pacitance of the stress sensors. The frequency f of the oscillator and the distance between the electrodes d have the following relationship

$$f = \frac{k}{RC} = \frac{k}{R(\varepsilon'S + C'd)}d \; , \qquad (6)$$

where ε' is the dielectric constant of the urethane foam, S is the area of the electrode, R is the feedback resistance, C' is the parasitic capacitance and k is a constant. When normal stress is applied to the stress sensor, as the Poisson's ratio of the urethane foam is nearly zero, oscillation frequency variation $\varDelta f$, variation $\varDelta d$ of d, and applied normal stress σ have the following relationship

$$\sigma = \frac{E}{d}\varDelta d = -\frac{Ek}{dR}\frac{(C'd + \varepsilon'S)^2}{\varepsilon'S}\varDelta f \; , \qquad (7)$$

where E is the Young's modulus of the urethane foam. Sensor outputs V_i in Fig. 3 correspond to frequency variation $\varDelta f_i$.
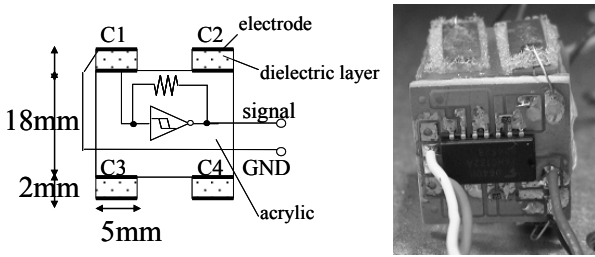

Fig. 5 Structure of the prototype

4.2 Setup

The cube was embedded in a silicone rubber as shown in Fig.6. Steel plates were placed at the top and bottom of the silicone. The top and bottom steel plates were moved in the z- and x-direction, respectively. In this experiment, as the boundary condition of the side was free, we assumed $\sigma_{xx} = 0$. Although the discussion was based on stress in Section.2, the experiment was based on displacement that we assume proportional to the stress.
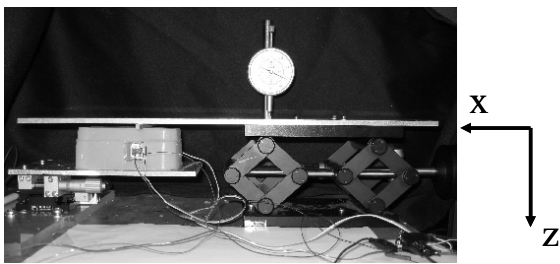

Fig. 6 Experimental setup

4.3 Amount of characteristic and experiments

We define P_{normal} proportional to the surface normal stress applied σ_{zz}, P_{shear} proportional to the shear stress σ_{zx} applied to the surface, and P_{grad} proportional to the gradient of the normal stress, $\partial \sigma_{zz}/\partial x$, as follows.

$$P_{normal} = -\varDelta f_1 - \varDelta f_2 - \varDelta f_3 - \varDelta f_4 \qquad (8)$$

$$P_{shear} = -\varDelta f_1 + \varDelta f_2 + \varDelta f_3 - \varDelta f_4 \qquad (9)$$

$$P_{grad} = \varDelta f_1 - \varDelta f_2 + \varDelta f_3 - \varDelta f_4 \qquad (10)$$

Due to the assumption $\sigma_{xx} = 0$, the x-direction components corresponding to $V_{5,6,7,8}$ are unnecessary.

First, only the top plate was moved in the z-direction. Fig. 7 (a) shows the results. The horizontal axis represents the displacement of the top steel plate. The vertical axis represents the calculated value of P_{normal}, P_{shear} and P_{grad}. As shown in Fig. 7 (a), while P_{normal} increases as the displacement in the z-direction increases, P_{shear} and P_{grad} don't seem to have such tendencies though small fluctuations can be seen.

Second, after the silicone was initially strained by moving the top plate in the z-direction up to 3 mm, only the bottom plate was moved in the x-direction. In this case, it is assumed that shear stress was uniformly applied on the top and bottom surface of the silicone rubber. Fig. 7 (b) shows the results. The horizontal axis represents the displacement of the bottom steel plate. As shown in Fig.7 (b), P_{shear} increases as the displacement in the x-direction increases, while P_{grad} does not seem to have such tendencies though small fluctuations can be seen. The reason that P_{normal} decreases is considered that the stationary z-direction strain is lighten up by the large shear deformation of the silicone.

At last, in order to apply normal stress non-uniformly on the surface of the silicone rubber, a square rod with the width of 5 mm was placed between the top steel plate and the surface of the silicone rubber. The x coordinate of the center of the square rod agreed with that of the capacitive displacement sensor C_2. The bottom plate was fixed and only the top plate was moved in the z-direction in this case. The results are shown in Fig. 7 (c). P_{grad} increases as the displacement in the z-direction increases, as we expected. However, P_{shear} also shows a similar tendency. The possible explanation for the results is that the point-spread pattern of normal stress distribution does not satisfy the assumption of the symmetry.

5. SUMMARY

We proposed a tactile sensing cube that is embedded in an elastic body and can measure the stress tensor around it. The theory to decompose the shear stress and the normal stress gradient is given. The theory was examined by a prototype sensor. Though the experimental results were not sufficient for fully supporting our proposed principle, the prototype exhibited different responses to the uniformly applied normal stress, the non-uniformly applied normal stress, and the uniformly applied shear stress. We are improving the experimental setup for more precise evaluation. In the future, the electrical power of the sensors and the data signals will be transmitted without complicated and long wires [3].
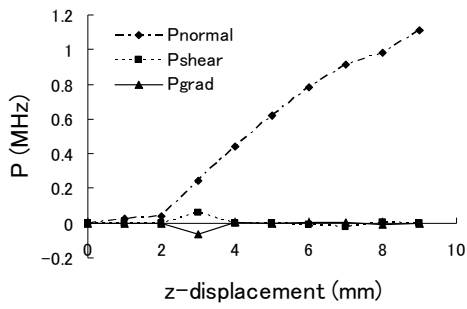
（a）
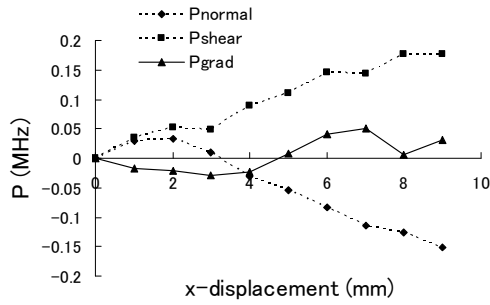
（b）
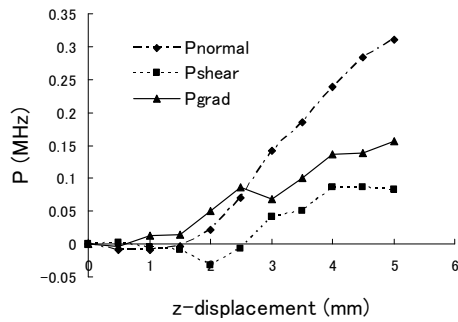
（c）

Fig. 7 Experimental results. (a): Normal stress was uniformly applied. (b): Shear stress was uniformly applied. (c): Linearly varied distribution of normal stress was applied.

REFERENCES

[1] M. H. Lee and H. R. Nicholls, "*Tactile sensing for mechatronics --a state of the art survey* ", Mechatronics 9 (1999), pp.1-31.

[2] H. Shinoda, K. Matsumoto and S. Ando, "*Acoustic Resonant Tensor Cell for Tactile Sensing*", Proceedings of the 1997 IEEE International Conference on Robotics and Automation Albuquerque, New Mexico - April 1997, pp. 3087-3092.

[3] Y. Makino, H. Chigusa and H. Shinoda, "Two Dimensional Sensor Integration Using Resonant Proximity Connector -Basic Technology and Application to Elastic Interface Device-," Proc. 3rd International Conference on Networked Sensing Systems (INSS 2006), pp. 196-202, 2006.